

DOCTORAL THESIS

---

# Thesis Title

---

*Author:*

Ana ANDRES-ARROYO

*Supervisor:*

Dr. First LAST

A thesis submitted in fulfilment of the requirements for the degree of  
Doctor of Philosophy



School of Physics, Faculty of Science

July 2018



*Dedicated to someone.*



*“Fancy Quote”*

Author



# Abstract

School of Physics, Faculty of Science, UNSW Australia

Doctor of Philosophy

**Thesis Title**

by Ana ANDRES-ARROYO

Write your abstract here .

# Acknowledgements

The acknowledgements and the people to thank go here, don't forget to include your project advisor...



# Contents

<b>Dedicatory</b>	<b>iii</b>
<b>Quotation</b>	<b>v</b>
<b>Abstract</b>	<b>vii</b>
<b>Acknowledgements</b>	<b>viii</b>
<b>Contents</b>	<b>ix</b>
<b>List of Figures</b>	<b>xi</b>
<b>Abbreviations</b>	<b>xiii</b>
<b>Physical Constants</b>	<b>xv</b>
<b>Symbols</b>	<b>xvii</b>
<b>1 Introduction</b>	<b>1</b>
1.1 Section title . . . . .	2
1.2 Compiling instructions . . . . .	2
1.3 References . . . . .	2
<b>2 Fourier transform as measurement of radial velocity</b>	<b>3</b>
2.1 Fourier transform as measurement of line shift . . . . .	4
2.1.1 Translation property of Fourier transform . . . . .	4
2.1.2 Intuitive explanation . . . . .	4
2.1.3 How to use . . . . .	5
Concluding remarks . . . . .	5
2.1.4 Sanity check . . . . .	6
Concluding remarks . . . . .	7
2.2 Fourier transform as measurement of line deformation . . . . .	8
2.2.1 Theory . . . . .	8
2.2.2 SOAP Simulations . . . . .	9
2.2.3 Jitter model . . . . .	11
2.2.4 Sanity check . . . . .	12
2.2.5 End-to-end Simulations . . . . .	13
2.3 Fourier transform with real observations . . . . .	16

2.3.1	HD189733: Rossiter–McLaughlin effect as jitter . . . . .	16
	Remarks . . . . .	17
2.3.2	Examples 2 . . . . .	17
2.3.3	Example 3 . . . . .	17
2.4	References . . . . .	19

# List of Figures

<b>1</b>	<b>Introduction</b>	<b>1</b>
<b>2</b>	<b>Fourier transform as measurement of radial velocity</b>	<b>3</b>
2.1	Translation property of Fourier transform . . . . .	6
2.2	Shifted line profile . . . . .	7
2.3	Fourier transform of shifted line profile . . . . .	7
2.4	Radial velocity recovery . . . . .	8
2.5	Deformed line profile . . . . .	10
2.6	Fourier transform of deformed line profile . . . . .	10
2.7	Fourier transform in response to line deformation . . . . .	11
2.8	Jitter model . . . . .	13
2.9	Corner plots of MCMC . . . . .	14
2.10	Planet recovery . . . . .	15
2.11	Distribution of recovered parameters . . . . .	16
2.12	Demo: Rossiter–McLaughlin effect . . . . .	17
2.13	From $RV_{\text{Gaussian}}$ and $RV_{\text{FT}}$ to $\Delta RV$ . . . . .	18
2.14	Rossiter–McLaughlin effect as jitter . . . . .	18



# Abbreviations

**2D** Two-Dimensional

**3D** Three-Dimensional



# Physical Constants

Speed of Light                       $c$     =     $2.997\,924\,58 \times 10^8 \text{ ms}^{-\text{s}}$  (exact)

Constant Name    Symbol    =    Constant Value (with units)





# Symbols

$f$	focal length	mm or cm
$H$	heating	K/W
$I$	intensity	a.u.
$k$	trap stiffness	pN/ $\mu$ m/mW
$n$	refractive index	—
$P$	power	mW
$T$	temperature	$^{\circ}$ C or K
$\varepsilon$	permittivity	???
$\kappa$	trap stiffness	pN/ $\mu$ m/mW
$\lambda$	wavelength	nm
$\mu$	permeability	???
$\sigma$	cross section	???
$\theta$	tilt angle	degrees or radians



# <sup>1</sup>Chapter 1

## Introduction

---

1.1	Section title . . . . .	2
1.2	Compiling instructions . . . . .	2
1.3	References . . . . .	2

## 1.1 Section title

Always put labelthsection after each section so the page headers work. [1]

This is a test.

## 1.2 Compiling instructions

1. make the main file the masted document: options -i make current file masted document
2. Quick build from anywhere (because it quick builds from the master document
3. BibTex from the chapter file (disable the master document option for this and do it from "normal mode")
4. Quick build 3 times (from the master document): 1 for the text, 2 for the references and labels, 3 for the bibliography backreferencing.

## 1.3 References

- [1] D. Selmeczi, S. F. Tolic-Norrelykke, E. Schaffer, P. H. Hagedorn, S. Mosler, K. Berg-Sorensen, N. B. Larsen, and H. Flyvbjerg. Brownian motion after einstein and smoluchowski: Some new applications and new experiments. *Acta Physica Polonica B*, 38(8):2407–2431, 2007. Cited in pages: 2

## <sup>1</sup> Chapter 2

# Fourier transform as measurement of radial velocity

---

<b>2.1</b>	<b>Fourier transform as measurement of line shift . . . . .</b>	<b>4</b>
2.1.1	Translation property of Fourier transform . . . . .	4
2.1.2	Intuitive explanation . . . . .	4
2.1.3	How to use . . . . .	5
	Concluding remarks . . . . .	5
2.1.4	Sanity check . . . . .	6
	Concluding remarks . . . . .	7
<b>2.2</b>	<b>Fourier transform as measurement of line deformation . . . . .</b>	<b>8</b>
2.2.1	Theory . . . . .	8
2.2.2	SOAP Simulations . . . . .	9
2.2.3	Jitter model . . . . .	11
2.2.4	Sanity check . . . . .	12
2.2.5	End-to-end Simulations . . . . .	13
<b>2.3</b>	<b>Fourier transform with real observations . . . . .</b>	<b>16</b>
2.3.1	HD189733: Rossiter–McLaughlin effect as jitter . . . . .	16
	Remarks . . . . .	17
2.3.2	Examples 2 . . . . .	17
2.3.3	Example 3 . . . . .	17
<b>2.4</b>	<b>References . . . . .</b>	<b>19</b>

*CGT: This needs a bit more helpful an introduction. That is WHY the fourier trasform is being explored as a way to measure radial velocity. and specifically, so that you can try to tell the difference between bulk line shifts, and line profile deformations. I think the folloing does a slightly better job of that.*

This chapter introduces a new method for measuring radial velocities. Specifically, it uses the Fourier transform of a line profile (or cross-correlation profile) to try and distinguish between the effects of a bulk shift in that profile (i.e. a radial velocity shift of the profile), and a change opposed to a change in the line profile shape which can produce an apparent radial velocity shift. We examine the impact on the Fourier transformed components of a line profile of both bulk line shifts, and line profile deformations, with the aim of developing tools to distinguish between these two cases.

## 2.1 Fourier transform as measurement of line shift

### 2.1.1 Translation property of Fourier transform

The translation of a function (in our case a spectral line profile) can be examined in both its original real space, and in its Fourier transformed space. Because Fourier techniques are often used to handle time domain data, this shift in real space can be variously considered described as either time shifting or translation. In this chapter we will refer to “time shifting”, “translation” and “velocity shifting” interchangeably to refer to a shift of a function in real space. We will refer to Fourier transformed functions as being in the “frequency domain” regardless of whether they have actual dimensions of 1/length or 1/velocity.

Let us consider a function  $h(x)$  be a signal  $f(x)$  delayed (or shifted) by an amount  $x_0$ :

$$h(x) = f(x - x_0). \quad (2.1)$$

In the frequency domain, we will then have

$$\hat{h}(\xi) = e^{-2\pi i x_0 \xi} \hat{f}(\xi), \quad (2.2)$$

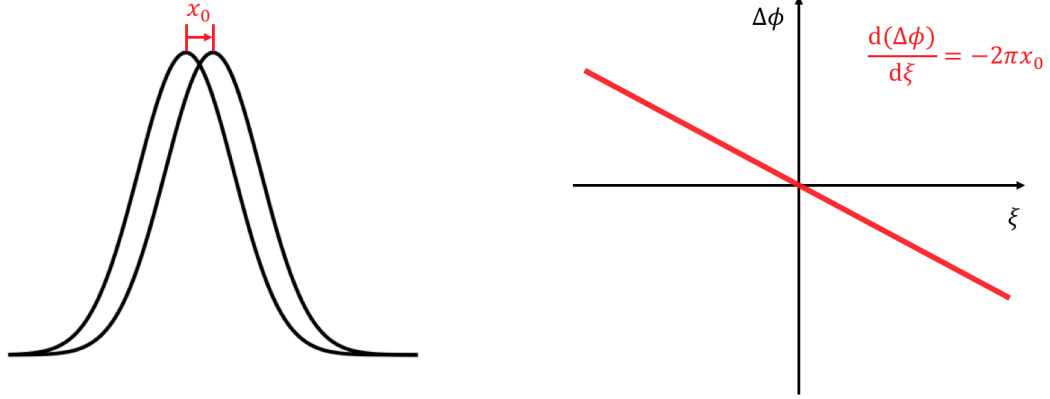


**Fig. 2.1:** The left panel shows a signal (or a spectral line profile in the following context) shifted by an amount  $x_0$ . The right panel is the differential phase spectral density diagram (i.e. differential phase spectrum). The model shows a perfectly linear correlation between  $\Delta\phi(\xi)$  and  $\xi$  with the constant slope  $-2\pi x_0$ .

where the circumflex denotes the Fourier transform of a function.  $\hat{h}(\xi)$  and  $\hat{f}(\xi)$  will therefore differ by a frequency dependent phase angle  $\Delta\pi$

$$\Delta\phi(\xi) = -2\pi x_0 \xi, \quad (2.3)$$

while the power spectral density will remain unchanged (as  $|e^{-2\pi i x_0 \xi}|^2 = 1$ ).

### 2.1.2 Intuitive explanation

The translation property of the Fourier transform follows mathematically from the nature of the transform. A (perhaps) more intuitive way to see this is that since the Fourier transform is defined

$$\hat{f}(\xi) = \int_{-\infty}^{\infty} f(x) e^{-2\pi i x \xi} dx, \quad (2.4)$$

it decomposes the function  $f(x)$  into a frequency representation  $\hat{f}(\xi)$ , such that the function is expressed as the sum of *all* over the orthogonal basis  $e^{2\pi i x \xi}$  of that basis times a set of components (i.e. by the inverse Fourier transform):

$$f(x) = \int_{-\infty}^{\infty} \hat{f}(\xi) e^{2\pi i x \xi} d\xi. \quad (2.5)$$

This means that shifting  $f(x)$  by  $x_0$  is equivalent to shifting *all* the orthogonal basis functions by  $x_0$ , which becomes  $e^{2\pi i(x-x_0)\xi}$ . This is how the  $e^{-2\pi i x_0 \xi}$  term in equation 2.2 arises comes along – it quantifies this phase difference.<sup>1</sup>

The fact that the power spectrum density remains the same can also intuitively seen, because shifting the signal as a whole doesn't add or remove any frequency information.

### 2.1.3 Practical Use

From Eq. 2.3, we see that the phase shift  $\Delta\phi(\xi)$  is proportional to the frequency  $\xi$  with a constant gradient or slope of  $\frac{d(\Delta\phi)}{d\xi}$

$$\frac{d(\Delta\phi)}{d\xi} = -2\pi x_0 \quad (2.6)$$

Obtaining this(in principle) straightforward via a simple linear regression model fit to a plot of  $\Delta\phi(\xi)$  versus  $\xi$  (see e.g. Fig. 2.1), so that

$$x_0 = -\frac{\frac{d(\Delta\phi)}{d\xi}}{2\pi} \quad (2.7)$$

By analogy with the definition of power spectral density, we describe  $\phi(\xi)$  the “phase spectral density” and hence  $\Delta\phi(\xi)$  the “differential phase spectral density”.

**Concluding remarks** In principle then, an analysis of the phase shift in the frequency domain of the Fourier components of a line profile will provide a means of measuring a bulk line shift in real space. More importantly, it may provide a means of separating an apparent radial velocity shift into the components due to bulk line shift, and line profile shape change.

---

<sup>1</sup>For a simplified vision bridging a shift of the signal in the time domain and a phase difference in the frequency domain, imagine any real continuous function is a sum of sines and cosines. Changing the phase angle in the sines and cosines results in shifts in the function.



### 2.1.4 Initial Tests check

We performed an initial test to determine whether we can correctly recover known shifts of a line profile from an analysis of the phase shift in the frequency domain of the Fourier transform of shifted line profiles.

We generated a spectral line profile based on the cross-correlation function of observed HARPS spectra with the software SOAP 2.0 *CGT: Referece*. This was replicated 100 times, with a very small amount of noise (equivalent to a S/N=10,000 in the line profiles) injected. These profiles were then subjected to radial velocity shifts evenly spaced between 0 and 10 m/s (Fig. 2.2).

The Fourier transform of these 100 spectral line profiles divides n them the information into two parts: (1) the power spectra (Fig. 2.3a) and (2) the phase spectra (shown in Fig. 2.3b as the differential phase spectra relative to the phase spectrum for the unshifted line profile).

*CGT: whereas the frequency ranges plotted in 2,.2a and 2.2b are the same [are they really? are you sure the axis on 2.2b should not be in m/s instead of km/s?] , the ranges plotted in 2.3a and 2.3b are different. You don't really say why. Until later when you make comments about "noise". I suggest you should make both the plots over the same range, and then \*point out\* the impact of noise, and why you have chosen to limit your fits to a smaller frequency range (and justify that choice),*

Most of the information in the power spectrum is concentrated in the lower frequency range in the power spectrum. As expected, the differential phase spectra are (by eye) linear <sup>2</sup>.

The slope of each differential phase spectrum indicates the shift of each line profile relative to the unshifted line profile. We therefore calculate the radial velocity shift for each shifted line profile using two methods: (1) the  $RV_{FT}$  from Eq. 2.7 and (2) the  $RV_{Gaussian}$  as traditionally measured from the line centroid by fitting a Gaussian to each line profile. We can then compare with with the (known) input line shift (Fig. 2.4) where we see the expected strong 1:1 correlation. The root-mean-square (rms) of the residuals are  $rms_{FT} = 0.13$  m/s and  $rms_{Gaussian} = 0.09$  m/s, indicating the expected radial velocities are cosistently reduced. *CGT: How do these comare which what you'd expect from the S/N and the intrinsic line width (should say at some int what the intrinsic line width is.*

---

<sup>2</sup>The slight deviation from linearity may come from the noise that we injected.

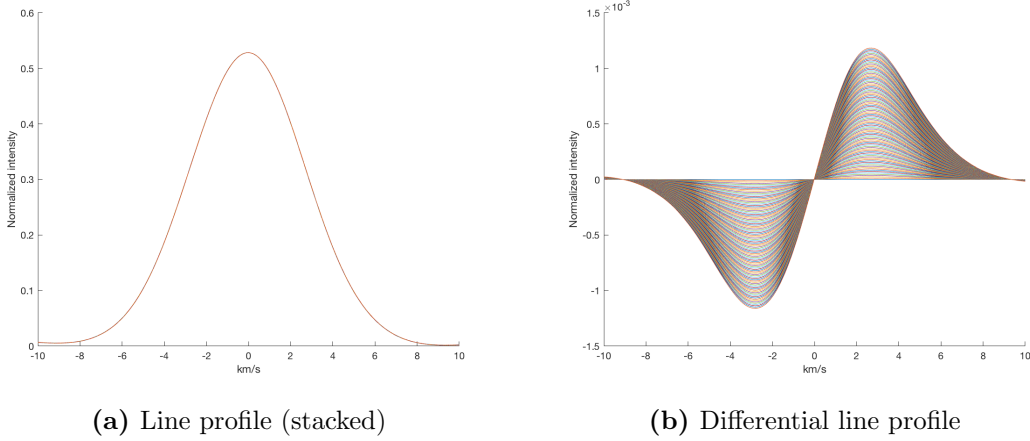


**Fig. 2.2:** (a) the shifted line profiles plotted on top of each other, showing how the  $\pm 0-10$  m/s shifts are very small compared to the line profile width. (b) the shifted line profiles with the unshifted line profile subtracted from each. Note that for clarity, noise is not included in this differential line profile plot.

Note that  $rms_{\text{FT}}$  is slightly larger than  $rms_{\text{Gaussian}}$ . This is because we only use part of the information from the original line profile – both because we utilise a limited range of the differential phase spectra, and because we use only the phase spectra to measure this shift (ignoring the power spectra), while the total information in the original shifted line profile is contained in the combination of the power and phase spectra.

*CGT: This needs more work. You need to show the region you are not using to explain why you choose a more limited range, and then say why you chose that more limited range and justify it. Don't just say "higher frequency".*

In fact, higher frequency range becomes useless as the interpretation of Fourier transform in high frequencies is dominated by noise and does not represent the intrinsic shift of the line profile any more. As a result, linearity of phase spectrum breaks down in higher frequencies. The range of “useful” frequencies will depend on the amount of noise (i.e. S/N).

**Concluding remarks** These initial tests confirm our expectation – it is possible to measure a radial velocity from the Fourier phase spectrum, and this provides an alternative to the traditional means of obtaining the radial velocities via centroiding the line profile in real space. In a broader context, this method will be applicable to measuring shifts of any pattern, and can be extended to higher dimensions. In this thesis, we primarily focus on its use to measure radial velocity shifts in spectral line profiles,

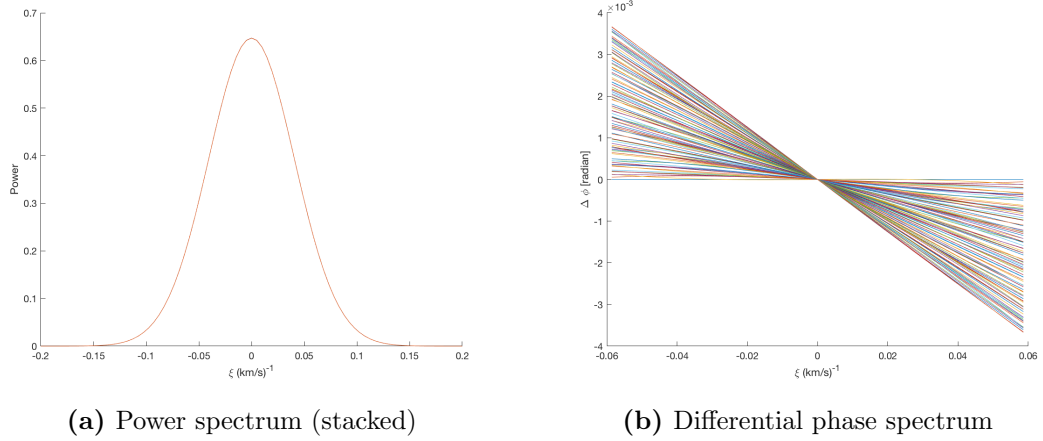


**Fig. 2.3:** The Fourier transform of these shifted line profile divides the information in each into (a) their power spectra and (b) their phase spectrum (here plotted differential compared to that of the unshifted profile). A line shift in the time domain produces an unchanged power spectrum in the frequency domain. It does, however, produce phase shift which we see as linear trends in the (differential) phase spectra as a function of frequency.

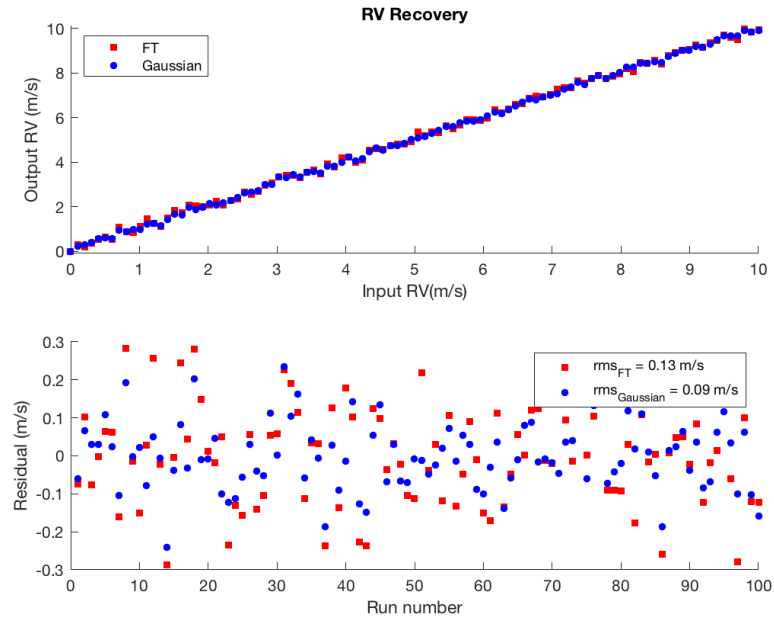


**Fig. 2.4:** Radial velocity recovery of line shifts

and especially whether the Fourier transform phase velocity is more robust against the influence of changes in line deformation than traditional techniques.

## 2.2 Using the Fourier transform to probe line deformation

### 2.2.1 Theory

We wish to test whether this new method for measuring radial velocities is more robust against spurious apparent radial velocity shifts produced by changes in the line profile shape in an emitting stars, rather than actual line profile shifts due to a bulk motion of the emitting star. In § 2.1, the same shift  $x_0$  applies to *all* the basis functions. In the case of line deformation due to stellar variability,  $x_0$  becomes frequency dependent<sup>3</sup>. That is to say, basis functions at different frequencies would shift by different amounts, resulting in shape changes (e.g. skewness) in the line profile. Therefore we modify the translation property of Fourier transform by rewriting  $x_0$  as  $x_0(\xi)$  in Eq. 2.3:

$$\Delta\phi(\xi) = -2\pi x_0(\xi)\xi. \quad (2.8)$$

As a result, the local gradient of the differential phase spectrum becomes

$$\frac{d(\Delta\phi)}{d\xi} = -2\pi(x_0 + \frac{dx_0}{d\xi}), \quad (2.9)$$

which reduces to Eq. 2.6 when  $x_0$  is a constant as in the case of a bulk line shift. Note that the dependency of  $\xi$  has been taken out of  $\Delta\phi(\xi)$  and  $x_0(\xi)$  in writing the differential equation above.

In principle, we could numerically solve this differential equation based on the measured local gradient  $d(\Delta\phi)/d\xi$  to obtain  $x_0(\xi)$ . As a simplistic approach, if  $x_0(\xi)$  changes with  $\xi$  slowly within a certain frequency range, we can make the approximations that  $x_0 \sim \text{const}$  and  $dx_0/d\xi \sim 0$ . With this, Eq. 2.9 converges back to Eq. 2.6.

### 2.2.2 SOAP Simulations

With SOAP 2.0, we inject three spots with different longitudes, latitudes and sizes (Table 2.1) to model an emitting star, and generate 100 cross-correlation functions for

---

<sup>3</sup>excluding the case where the result of a line deformation is exactly the same as a line shift, as this becomes indistinguishable by any means

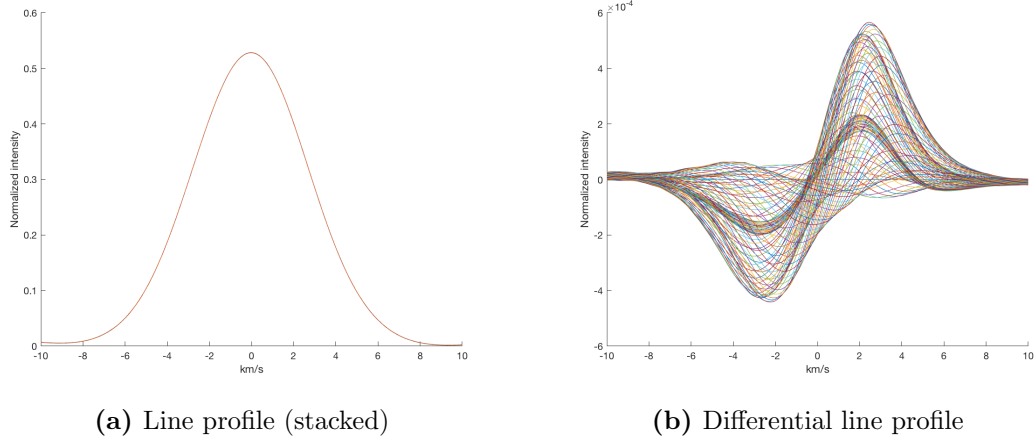


**Fig. 2.5:** Deformed line profile. For the sake of clarity, noise is not included in this differential line profile plot.

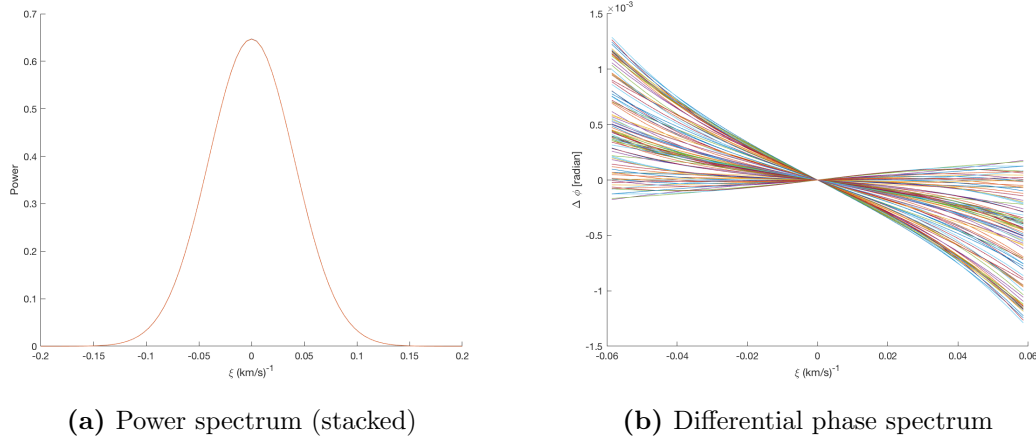


**Fig. 2.6:** Fourier transform of deformed line profile.

the resulting deformed line profiles evenly sampled throughout the rotation period of the star (Fig. 2.5). We then take the same approach as in § 2.1.

	Longitude	Latitude	Size in disk area percentage
Spot 1	174°	-14°	0.18%
Spot 2	288°	74°	0.40%
Spot 3	51°	52°	0.50%

**Table 2.1:** Spot configurations

If we compare the differential phase spectra in Fig. 2.3 and Fig. 2.6, it is quite obvious that the differential phase spectrum of a deformed line profile is no longer linear due to the  $x_0$  dependency on  $\xi$ , as we discussed in § 2.2.1. Nevertheless, applying the

local linear approximation can provide a radial velocity shift for that frequency range. We will primarily use the lower frequency range (from  $-0.06$  to  $0.06 \text{ (km/s)}^{-1}$  in this case) for the reasons that it is where information is mostly concentrated and that it is less noise-sensitive. *CGT: Sorry, but you still haven't demonstrated this sufficiently*

We find, to our surprise, that  $RV_{\text{FT}}$  is linearly correlated with  $RV_{\text{Gaussian}}$ , with a slope  $k$  close to, but different from, unity –  $k \sim 0.84$  (Fig. 2.7). *CGT:  $k$  never defined anywhere.* The non-zero slope indicates that the intrinsic line deformation (in the absence of any velocity shift in the host star) does (as expected) mimic a the radial velocity shift.

However, the differential phase shift at lower frequency is *less* sensitive to the influence of line profile deformation. If we concentrate on frequencies in the range  $|\xi| < 0.06 \text{ (km/s)}^{-1}$  (sensitive to line profile structure at velocities  $> 1/|\xi| = 16 \text{ km/s}$ ) we find that these lower frequency modes are less effectively modulated by the higher frequency line deformations, as shown in the differential line profile in Fig. 2.5b.

In addition, the slope  $k$  will change depending on the frequency range in which the linear regression model is applied. For example, if we select the higher frequency range in the differential phase spectrum, we will expect larger  $RV_{\text{FT}}$  and hence a larger  $k$  in general.

*CGT: I tried to rewrite the above, but I'm not convinced either the text or the figures are very clear! In partiucular you need a clear and compelling demosntration why you've chosen the lower frequency range you have*

### 2.2.3 Jitter model

We have found in § 2.1 that  $RV_{\text{FT}}$  and  $RV_{\text{Gaussian}}$  demonstrate basically the same response to radial velocity shifts. We have also found in section (§ 2.2) that  $RV_{\text{FT}}$  in the lower frequency range *CGT: What range compared to, say, the line width of the line profile?* is less sensitive to line deformation than  $RV_{\text{Gaussian}}$ , as the correlation between  $RV_{\text{FT}}$  and  $RV_{\text{Gaussian}}$  is linear with a slope  $k$  less than 1 by between 15-20%.

We can therefore write the following measurable quantities –  $RV_{\text{FT}}$  and  $RV_{\text{Gaussian}}$  – as the sum of corresponding contributions from a bulk shift in the star (which we hereafter assume to be due to a planet or planets), and variability in the stellar line

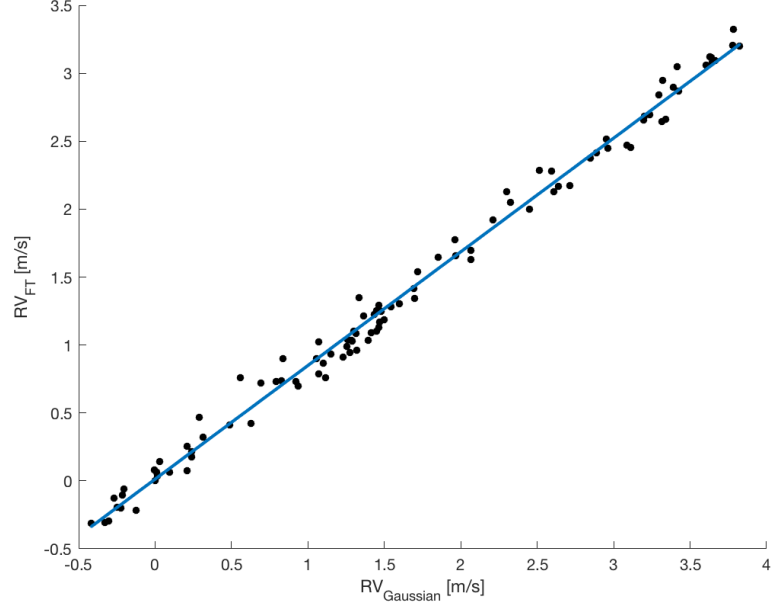


**Fig. 2.7:**  $RV_{\text{FT}} \sim k \cdot RV_{\text{Gaussian}}$  ( $k < 1$ )

profile (hereafter lumped under the general name “jitter”):

$$RV_{\text{Gaussian}} = RV_{\text{planet}} + RV_{\text{jitter}} \quad (2.10)$$

and

$$RV_{\text{FT}} = RV_{\text{planet}} + k \cdot RV_{\text{jitter}}. \quad (2.11)$$

Subtracting one from the other to remove  $RV_{\text{planet}}$  gives

$$\Delta RV = (1 - k) \cdot RV_{\text{jitter}} \quad (2.12)$$

where  $\Delta RV = RV_{\text{Gaussian}} - RV_{\text{FT}}$ . Rearranging yields

$$RV_{\text{jitter}} = \alpha \cdot \Delta RV \quad (2.13)$$

where  $\alpha = 1/(1 - k)$  is a scaling factor.

#### 2.2.4 Testing the recovery of Jitter

We will again perform a sanity check to see if we can correctly recover artificially generated model jitter using our new technique (Eq. 2.13).

To start with, we generate 200 deformed line profiles (in the form of cross-correlation functions) with SOAP 2.0. All the configurations are the same as §2.2.2 except that they are evenly sampled throughout two rotation periods. The jitter amplitude is roughly 2 m/s. In addition, each line profile is further shifted by an amount  $RV_{\text{planet}}$ , of which the amplitude

$$A_{\text{planet}} = 2 \text{ m/s}$$

and the planetary orbital frequency to stellar rotation frequency ratio

$$\frac{\nu_{\text{orb}}}{\nu_{\text{rot}}} = \frac{P_{\text{rot}}}{P_{\text{orb}}} = 0.7.$$

In fact, the  $RV_{\text{planet}}$  configuration shouldn't matter much because it will be mostly cancelled out in the jitter model. We then obtain two sets of radial velocities:  $RV_{\text{Gaussian}}$  and  $RV_{\text{FT}}$ , as seen in the upper panel of Fig. 2.8. As we know the amount of input jitter in our simulation, we simply scale up  $\Delta RV$  by a parameter  $\alpha$  to match the input jitter (dashed line in middle panel). The jitter model (black dots in middle panel) becomes more scattered as  $\alpha \gg 1$ . As a result, a moving average modulated by a Gaussian kernel is implemented to smooth out the data (solid line in middle panel).

To comment on the performance, we compare the rms of the input jitter  $rms_{\text{jitter}}$  and the rms of the residual between the input jitter and the model jitter  $rms_{\text{residual}}$ . The former can be treated as the scatter after fitting the correct planet(s) without jitter correction, while the latter treated as the scatter after the additional jitter is removed. The rms is reduced from  $rms_{\text{jitter}} = 1.22 \text{ m/s}$  to  $rms_{\text{residual}} = 0.70 \text{ m/s}$ , which is crucial in enhancing the detection of planets with radial velocities of sub-m/s amplitudes. However, we should also note that there are systematic differences between the input jitter and our model jitter (i.e. the residual sorts of repeats itself in the two stellar rotation periods). We should be aware that while removing the stellar variability contribution from the data, it may also add in some remnant features.

## 2.2.5 End-to-end Simulations

Unless we are sure of a null-planetary system where  $RV_{\text{planet}} = 0$  and from Eq. 2.10 and Eq. 2.11 we obtain

$$k = RV_{\text{jitter}}/RV_{\text{Gaussian}}, \quad (2.14)$$



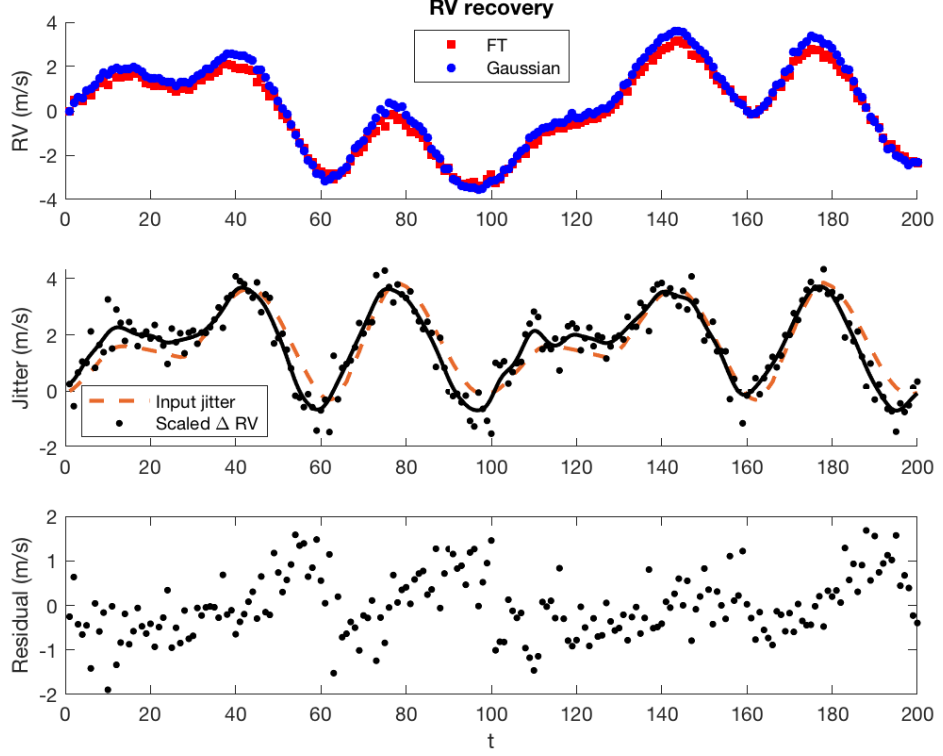


**Fig. 2.8:** Construct jitter model from simulation data.

normally  $k$  cannot be directly calculated, so neither can  $\alpha$  be. However, we could substitute the jitter model (Eq. 2.13) into Eq. 2.10, such that

$$RV_{\text{Gaussian}} = RV_{\text{planet}} + \alpha \cdot \Delta RV \quad (2.15)$$

where  $RV_{\text{planet}}$  is parametrised by Keplerian orbit(s) and both  $RV_{\text{Gaussian}}$  and  $\Delta RV$  are measurable.

The tests are divided into two groups for comparison:

1. Fit  $RV_{\text{Gaussian}}$  by Keplerian orbit alone;
2. Fit  $RV_{\text{Gaussian}}$  by Keplerian orbit + jitter model (i.e.  $\alpha \cdot \Delta RV$ ).

The injected planet has the same parameter settings as in §2.2.4, i.e. circular orbit with amplitude  $A = 2$  m/s, orbital frequency ratio  $\nu = 0.7$  and initial phase  $\omega = 1$  rad. We will compare which group recovers the planet parameters better.

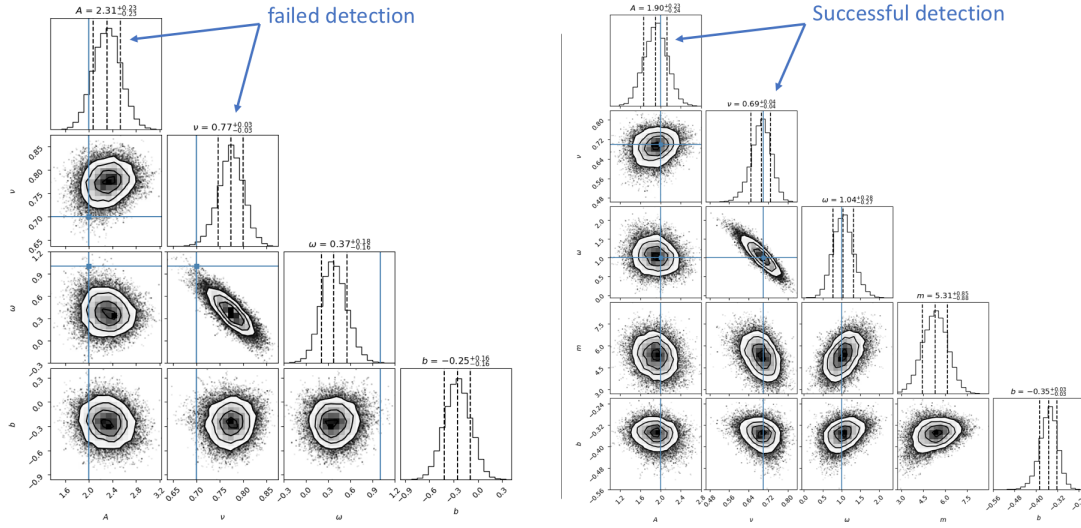


**Fig. 2.9:** Corner plots of MCMC. These are two examples of the output of MCMC: no jitter correction on the left and with jitter correction on the right. The input parameters are highlighted in the blue solid line. The three dashed lines of each histogram indicate the median and  $1\sigma$  on both sides. On the left panel both blue lines of  $A$  and  $\nu$  are outside the  $1\sigma$  region, therefore it counts as a “failed detection”; on the right panel, it counts as a successful detection within  $1\sigma$ .

To better simulate the real observations, 40 data samples out of 200 from the two rotation periods are randomly selected. The fitting is achieved by running MCMC to maximise the log-likelihood function given the model. For the simulation, each radial velocity data is equally weighted (as they have the same S/N). It is defined if the input parameter lies within  $1\sigma$  errorbar of the output parameter, it counts as a successful detection.

For demonstration, we show one of the outputs in corner plots (Fig. 2.9) and the corresponding radial velocity fitting (Fig. 2.10). The corner plot visually shows the how the walkers explore the parameter space and their distribution. The histogram gives an example explaining how a “successful detection” is qualified. The radial velocity fitting plot demonstrates an example that implementing the jitter model effectively accounts for the spurious signals in the raw radial velocity data, reducing the rms from 1.14 m/s to 0.55 m/s.

In the end, we run 100 trails for the end-to-end simulation. The random differences among these 100 trails come from:

- photon noise given the S/N;

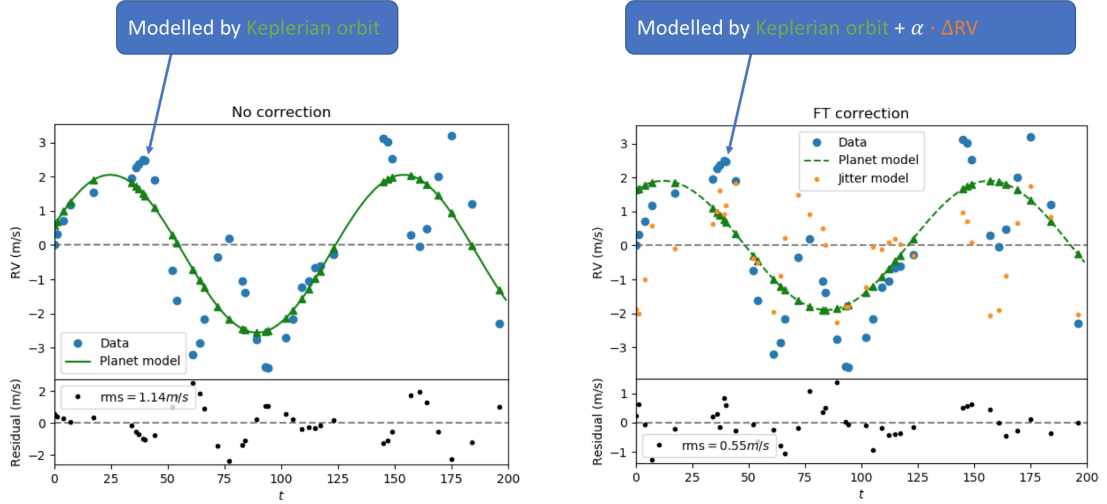


**Fig. 2.10:** Radial velocity fitting. These are two fittings that come out from the MCMC corner plots in Fig. 2.9. On the left panel without jitter correction, we can see that the input jitter increases the scatter of the raw radial velocities, resulting in an overestimated amplitude  $A$ ; while on the right panel with jitter correction, the additional input jitter is accounted for by the jitter model.

- randomly selected 40 samplings in the 200 line profiles.

It turns out that in 46% of the 100 trails are successful detections for both  $A$  and  $\nu$  when we apply the jitter correction model, while this percentage is only 11% without jitter correction. In more detail, Fig. 2.11 shows that with jitter correction (in red), both of the amplitude and orbital frequency ratio tend to be underestimated, which is shown opposite for the results without correction (in blue). Moreover, the jitter corrected parameters are better constrained (i.e. with narrower distributions) and performs much better in  $\nu$  than without correction. While it is tempting to say the correct answer is more likely in between the results from these two fittings, we would need more tests to conclude.

## 2.3 Fourier transform with real observations

### 2.3.1 HD189733: Rossiter–McLaughlin effect as jitter

HD189733 is a well studied binary star system. The main star HD189733 A is known to host a gas giant exoplanet HD189733 b, first detected by transits (reference...) and later

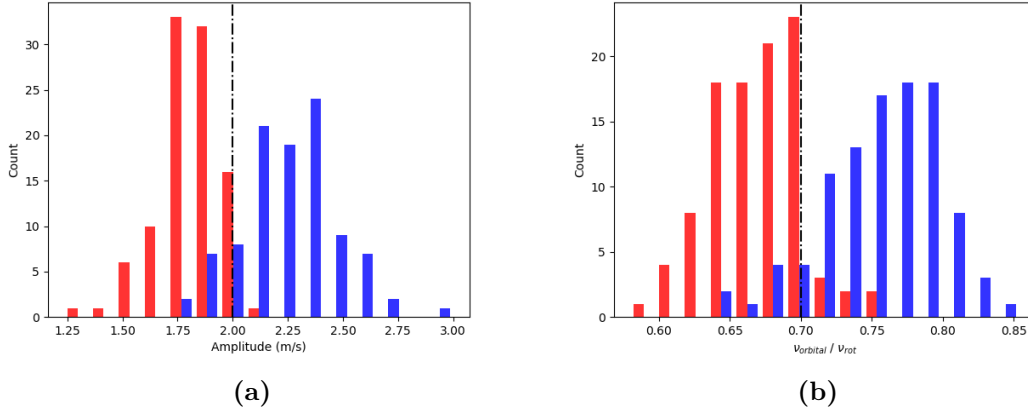


**Fig. 2.11:** Distribution of recovered parameters. The red are results of jitter correction by Fourier transform; The blue are results of no jitter correction.

by Doppler spectroscopy (references...). It was also the first exoplanet transit observed in X-ray (references...).

We choose this target for the following reasons:

- The exoplanet is well confirmed;
- The host star is bright enough:  $m_v = 7.66$
- The gas giant causes a prominent apparent radial velocity while it transits ( $\sim 40$  m/s) due to Rossiter–McLaughlin effect.

We treat as if it were an “active” star with one big dark starspot, as the Rossiter–McLaughlin effect causes the line profile deformed in a similar manner that a starspot would do (Fig. 2.12). We would see if our jitter model can account for the radial velocity variation from Rossiter–McLaughlin effect.

The procedure is rather standardized. Both  $RV_{\text{Gaussian}}$  and  $RV_{\text{FT}}$  are calculated from the HARPS cross-correlation functions of the spectra.  $\Delta RV = RV_{\text{Gaussian}} - RV_{\text{FT}}$  are then smoothed by a Gaussian filter (Fig. 2.13). The prototype of the Rossiter–McLaughlin radial velocity curve is already identifiable in  $\Delta RV$  of the lower panel.

To extract the Rossiter–McLaughlin radial velocity curve, a linear trend is fitted to account for the other binary star. After the linear trend is removed, it is treated as jitter and modelled by  $\alpha \cdot \Delta RV$  (Fig. 2.14). Note that the errorbars of the jitter model also becomes a factor of  $\alpha$  ( $\alpha \gg 1$ ) larger; however, the model itself shows a

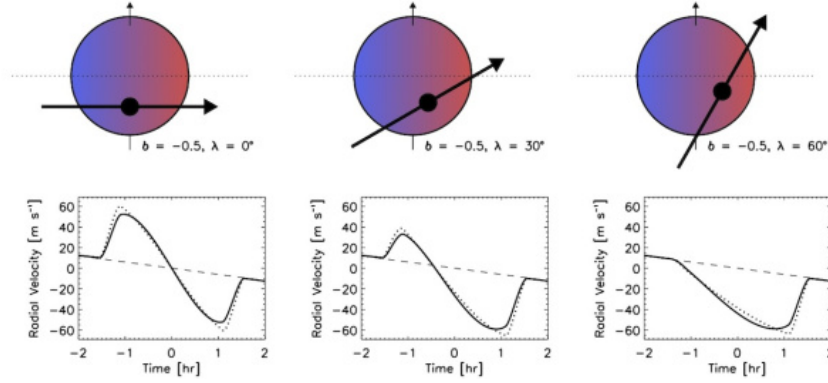


**Fig. 2.12:** Demo: Rossiter–McLaughlin effect (reference...). It is a apparent radial velocity change of the parent star due to an eclipsing binary (whether star or planet) that breaks the observed flux symmetry in the stellar photosphere, resulting in imbalanced redshift and blueshift. It shows in this plot three different star-planet alignments that causes three corresponding different shapes of radial velocity curve, and hence the radial velocity curve sheds information on the geometry of the alignment.

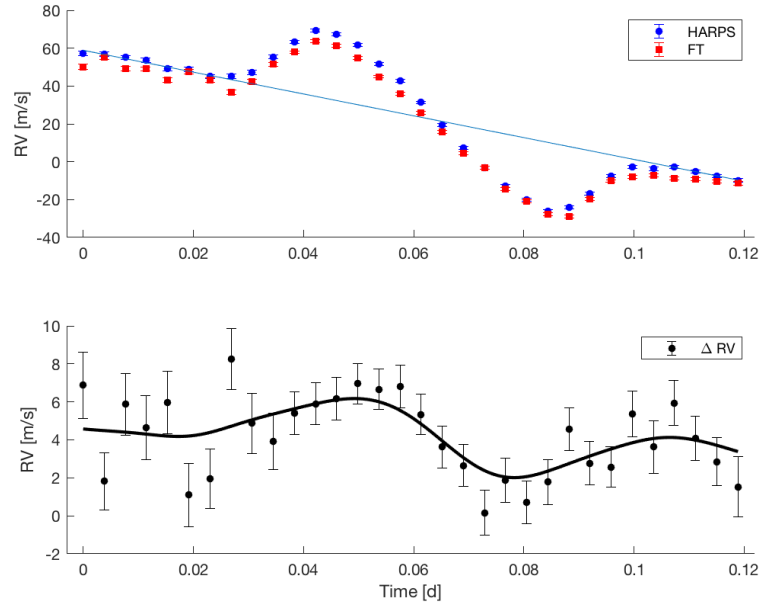


**Fig. 2.13:** From  $RV_{\text{Gaussian}}$  and  $RV_{\text{FT}}$  to  $\Delta RV$ . The scattered  $\Delta RV$  are smoothed by applying a moving average with a Gaussian filter and further weighted based on the size of errorbar.

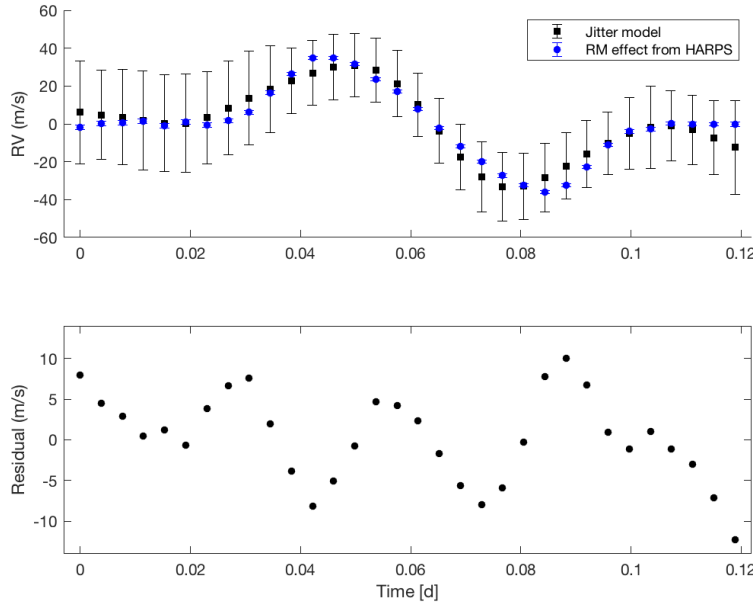


**Fig. 2.14:** Rossiter–McLaughlin effect as jitter fitted with the jitter model.

descent approximation of the Rossiter–McLaughlin radial velocity curve. The peak of the “jitter” is reduced from  $\sim 40$  m/s to  $\sim 10$  m/s.

**Remarks** The effective length of the smoothing kernel should be carefully chosen. In this case, it’s chosen most effective within roughly one neighbouring data point on both size. While mitigating the effect of noise (especially for relatively lower S/N data outside the transits), to which the Fourier transform is sensitive, it also smears the drastic velocity change when the planet ingresses and egresses the stellar disk. To solve this awkward situation, an adaptive (i.e. S/N dependent) effective length of the smoothing kernel may be used.

### 2.3.2 Examples 2

### 2.3.3 Example 3

A float barrier will stop figures from going beyond this point. They are handy to make sure they don’t go into the next section.

## 2.4 References

- [1] D. Selmeczi, S. F. Tolic-Norrelykke, E. Schaffer, P. H. Hagedorn, S. Mosler, K. Berg-Sorensen, N. B. Larsen, and H. Flyvbjerg. Brownian motion after einstein and smoluchowski: Some new applications and new experiments. *Acta Physica Polonica B*, 38(8):2407–2431, 2007. Cited in pages:

